coatings

MDPI

Article

Etching Processing of InGaAs/InAlAs Quantum Cascade Laser

Qi Wu [1,2,3,4], Yana Zhu [1,2,3,4], Dongxin Xu [1,2,3,4], Zaijin Li [1,2,3,4], Yi Qu [1,2,3,4,*], Zhongliang Qiao [1,2,3,4], Guojun Liu [1,2,3,4], Zhibin Zhao [1,2,3,4], Lina Zeng [1,2,3,4], Hao Chen [1,2,3,4] and Lin Li [1,2,3,4]

1 College of Physics and Electronic Engineering, Hainan Normal University, Haikou 571158, China; wuqihainan@163.com (Q.W.); 15607693682@163.com (Y.Z.); jilinchangchun@yeah.net (D.X.); lizaijin@hainu.edu.cn (Z.L.); qzhl060910@hainnu.edu.cn (Z.Q.); gjliu626@126.com (G.L.); 060111@hainnu.edu.cn (Z.Z.); zenglina@hainnu.edu.cn (L.Z.); 15948713468@163.com (H.C.); lin.li@hainnu.edu.cn (L.L.)
2 Hainan Provincial Key Laboratory of Laser Technology and Optoelectronic Functional Materials, Innovation Center of Hainan Academician Team, Haikou 571158, China
3 Hainan International Joint Research Center for Semiconductor Lasers, Hainan Normal University, Haikou 571158, China
4 Engineering Research Center of Laser Technology and Application of Hainan Province, Haikou 571158, China
* Correspondence: quyihainan@126.com

Abstract: The 3–5 μm mid-infrared band is the atmospheric window band, where there are absorption peaks of many molecules. It plays an important role in trace gas detection, directional infrared countermeasures, biomedicine, and free-space optical communications. The wet etching process of the designed InGaAs/InAlAs quantum cascade laser with superlattice structure was explored to provide a good experimental basis for the research and development of lasers. The HBr:HNO_3:H_2O series of etching solutions were selected for corrosion experiments, and the surface morphology was observed by scanning electron microscopy (SEM) and metallographic microscopy to obtain the corrosion rate of the etching solution. The experimental results show that the etching liquid ratio is HBr:HNO_3:H_2O = 1:1:10, and the etching rate is 0.6 μm/min. A quantum cascade laser that works continuously at room temperature was prepared, with an injection strip width of 7 μm, a cavity length of 4mm, and an operating temperature of 20 °C. The device works in continuous mode (CW), with a maximum continuous output power of about 186 mW, a threshold current of about 0.4 A, a threshold current density of about 1.428 kA/cm^2, a device center wavelength of about 4424 nm, a side mode suppression ratio of 28 dB, and a spectrum full width at half maximum of 2 nm.

Keywords: InGaAs/InAlAs; quantum cascade laser; etching process; corrosion rate; surface morphology

check for updates

Citation: Wu, Q.; Zhu, Y.; Xu, D.; Li, Z.; Qu, Y.; Qiao, Z.; Liu, G.; Zhao, Z.; Zeng, L.; Chen, H.; et al. Etching Processing of InGaAs/InAlAs Quantum Cascade Laser. *Coatings* **2024**, *14*, 1448. https://doi.org/10.3390/coatings14111448

Academic Editor: Michał Kulka

Received: 28 October 2024
Revised: 11 November 2024
Accepted: 12 November 2024
Published: 13 November 2024

Copyright: © 2024 by the authors. Licensee MDPI, Basel, Switzerland. This article is an open access article distributed under the terms and conditions of the Creative Commons Attribution (CC BY) license (https://creativecommons.org/licenses/by/4.0/).

1. Introduction

Quantum cascade laser (QCL) is a unipolar semiconductor laser that emits light by electron transitions between the conduction band and sub-band [1]. It is an important frontier in the realization of mid-infrared lasers in the 3–5 μm band. It has important application value in many fields [2], such as trace gas detection [3], directional infrared countermeasures [4], biomedicine [5], and free-space optical communication [6].

As early as 1995, Faist used a wet etching process to prepare a ridge waveguide with a ridge width of 9 μm [7], a QCL lasing wavelength of 4.6 μm, and an output power of about 2 mW under continuous operation at 85 K. In 2001, Hofstetter used a wet etching process (non-selective etching solution HBr:HNO_3:H_2O) to prepare a ridge waveguide with a ridge width of 44 μm and a lasing wavelength of 5.3 μm [8]. In 2004, Evans used a wet etching process to prepare a ridge waveguide with a ridge width of 12 μm [9], a lasing wavelength of 4.8 μm, and a continuous output power of about 370 mW. In 2005, Wang Zhanguo's team used a wet etching process (non-selective etching solution HBr:HNO_3:H_2O) to prepare a ridge waveguide with a ridge width of 20 μm [10]. In 2006, Slivken et al. used a wet

etching process to fabricate a ridge waveguide with a ridge width of 12 μm [11]. In 2007, Evans used a wet etching process (non-selective etching solution HBr:HCl:H_2O_2:H_2O) to prepare a ridge waveguide with a ridge width of 6 μm [12], a lasing wavelength of 4.7 μm, and a room temperature continuous output power of more than 0.675 W. In 2008, Bai used a wet etching process (non-selective etching solution HBr:HCl:H_2O_2:H_2O) to prepare a ridge waveguide with a ridge width of 9.8 μm [13], a device lasing wavelength of 4.6 μm, and a maximum room temperature continuous output power of 1.3 W. In 2011, Bai used a wet etching process (non-selective etching solution HBr:HCl:H_2O_2:H_2O) to prepare a ridge waveguide with a ridge width of 8 μm [14]. The room temperature continuous output power reached 5.1 W, making it the world's highest output power QCL. In 2013, Wang Zhanguo's team used a wet etching process to prepare a ridge waveguide with a ridge width of 9 μm [15] and a lasing wavelength of 4.7 μm. Under continuous working conditions at 15 °C, the device output power exceeded 0.85 W, and the threshold current density was 1.19 kA/cm^2. In 2022, Pang Lei et al. used a wet etching process to prepare a ridge waveguide with a ridge width of 13 μm [16]. The device lasing wavelength was 4.6 μm. At a temperature of 15 °C, the continuous output power was about 364 mW, and the threshold current density was about 1.04 kA/cm^2. In 2023, Liu Fengqi's team used wet etching (non-selective HBr:HNO_3:H_2O) to prepare a ridge waveguide with a ridge width of 7.5 μm [17]. The lasing wavelength was 4.6 μm, and the continuous output power could reach 3 W at a temperature of 11 °C.

The ridge waveguide table structure of the quantum cascade laser can be prepared by dry etching or wet etching. Bewley found that a ridge waveguide prepared by dry etching [18] had rough side walls, and there was surface recombination and current leakage, which made the threshold current of the QCL larger. The ridge waveguide prepared by wet etching had smooth side walls. Andreas found that after etching the sample with CH_3COOH:HCl:H_2O_2 = 5:5:1 etching solution [19], the mask corrosion was uneven, the etching side walls were rough, the lateral drilling phenomenon was serious, and a large number of defects appeared in the active area. In previously reported InGaAs/InAlAs material corrosion systems, the commonly used corrosion solutions are HCl:HNO_3:H_2O, HBr:HCl:H_2O_2:H_2O, HBr:HNO_3:H_2O, etc. Among them, the corrosion solution with the ratio of HCl + HNO_3 + H_2O in the hydrochloric acid system is too oxidizing, which has strong corrosiveness to the AZ5214 photoresist used as a mask, and it has poor surface morphology, which is not suitable for device preparation. The corrosion solution with the ratio of HBr + HCl + H_2O_2 + H_2O in the hydrobromic acid system will not corrode the AZ5214 photoresist, and the surface morphology is good, but HCl and H_2O_2 have strong oxidizing properties, the corrosion rate of the corrosion solution is fast, and the controllability is poor. The corrosion solution with the ratio of HBr + HNO_3 + H_2O in the hydrobromic acid system will not corrode the AZ5214 photoresist, the surface morphology is good, the etching rate is slow, and the controllability is good. Therefore, the quantum cascade laser reported in this paper focuses on the etching process of the double-channel ridge waveguide. The HBr:HNO_3:H_2O etching solution was used for the wet etching process, and a ridge waveguide table structure with smooth sidewalls could be obtained. The device has an injection strip width of 7 μm, a cavity length of 4 mm, and an operating temperature of 20 °C, and the device works in continuous mode (CW). The maximum continuous output power of the device is about 186 mW, the threshold current is about 0.4 A, the threshold current density is about 1.428 kA/cm^2, the device center wavelength is about 4424 nm, the side mode suppression ratio is 28 dB, and the spectrum full-width half maximum is 2 nm.

2. Principles and Experiments

2.1. QCL Working Principle

Conventional semiconductor lasers mainly rely on electrons in the role of the applied electric field from the conduction band under the action of transitioning to the valence band, resulting in electron–hole recombination luminescence. Figure 1a shows the schematic

diagram of the energy band structure of the conventional semiconductor laser. The conventional semiconductor laser excitation wavelength is mainly determined by the forbidden bandwidth (Eg) of the semiconductor materials, but the forbidden bandwidth of the semiconductor materials used is limited, limiting the excitation wavelength of the device. The quantum cascade laser is a kind of electron in the conduction band sub-band between the transition luminescence of the semiconductor lasers; it relies on a single carrier (electron) jump emitting light, breaking the limitations of the forbidden bandwidth of semiconductor materials, and it allows the excitation wavelength to be altered by artificially designing the thickness of the quantum well in the gain region. The energy band structure and working principle of the QCL is shown in Figure 1b. A single cycle of the QCL is composed of an injection region and an active region. The whole device gain region consists of n (10–100) cycle repetitions, in which the injection region is the region of injected electrons and the active region is the region of excited light. The transition luminescence of the electrons between the sub-bands occurs between the E_3 energy level and the E_2 energy level, and then the electrons rely on the longitudinal optical (LO) phonon resonance scattering mechanism to transition from the E_2 energy level to the E_1 energy level, at which time the electrons enter into the injection region of the next cycle, and through the resonance tunneling effect, they enter into the E_3 energy level of the active region of the next cycle, which satisfies the population inversion condition of the next process and carries out the next cyclic cascade of the radiative transition. Whereas these electrons are reused throughout the cycle, a single electron is capable of emitting n photons, which improves the utilization of electrons and increases the slope efficiency of the device.

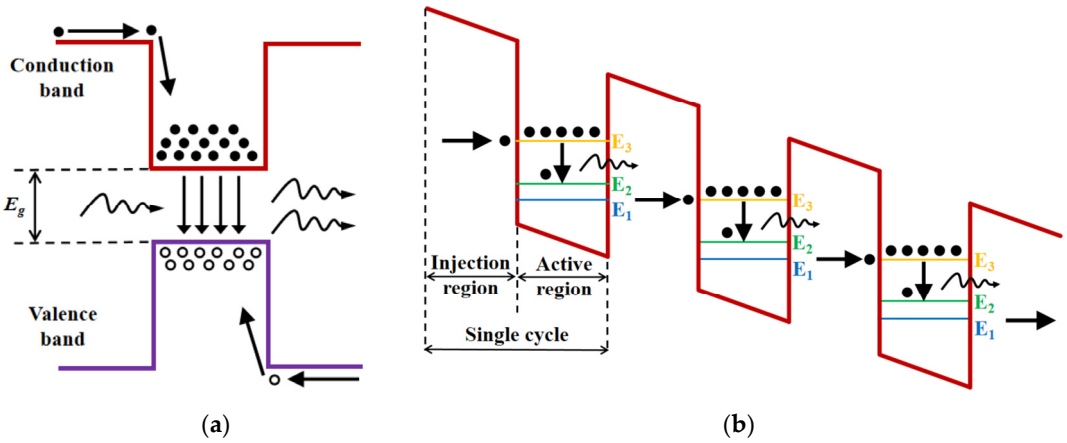

Figure 1. (**a**) The schematic diagram of the energy band structure of the conventional semiconductor laser; (**b**) the energy band structure and working principle of the quantum cascade laser.

2.2. QCL Epitaxial Structure

The QCL epitaxial structure was grown and prepared by the molecular beam epitaxy (VG, East Sussex, UK) process, and the epitaxial structure is shown in Table 1: the substrate is n-type Si-doped InP with a doping concentration of 3×10^{17} cm^{-3}; the lower cladding layer is 1350-nm-thick InP with a doping concentration of 2.2×10^{16} cm^{-3}; the upper and lower waveguide layers are both 300-nm-thick InGaAs with a doping concentration of 4×10^{16} cm^{-3}; the active region is 1410-nm-thick $In_{0.669}Ga_{0.331}As/In_{0.362}Al_{0.638}As$, in which part of the material in the active region has been doped with n-type Si, with a doping concentration of 2.5×10^{17} cm^{-3}. The purpose of the n-type Si doping is to provide the device with a sufficient free electron concentration to achieve effective carrier injection and improve device efficiency and stability; the upper cladding layer is 2600-nm-thick InP with a doping concentration of 3×10^{16} cm^{-3}; the gradually doped layer is 150-nm-thick InP with a doping concentration of 1~3×10^{17} cm^{-3}; the cap layer is highly doped 400-nm-thick InP with a doping concentration of 2×10^{19} cm^{-3}.

Table 1. Epitaxial structure of quantum cascade laser.

Number	Layers	Materials	Thickness (nm)	Doping(cm^{-3})
7	Highly Doped Layer	InP	400	n, Si, 2×10^{19}
6	Gradually Doped Layer	InP	150	n, Si, $1\sim3 \times 10^{17}$
5	Upper Cladding	InP	2600	n, Si, 3×10^{16}
4	Waveguide Layer	InGaAs	300	n, Si, 4×10^{16}
3	Active Region (×28)	$In_{0.669}Ga_{0.331}As/In_{0.362}Al_{0.638}As$	1410	
2	Waveguide Layer	InGaAs	300	n, Si, 4×10^{16}
1	Lower Cladding	InP	1350	n, Si, 2.2×10^{16}
	Substrate	InP	400	n, Si, 3×10^{17}

2.3. QCL Chip Process

The QCL chip process flow is shown in Figure 2. Firstly, the epitaxial wafer is cleaned by soaking in acetone (Xilong Scientific, Swatow, China) for 5 min to remove the surface oil, then cleaned with anhydrous ethanol (Xilong Scientific, Swatow, China) and deionized water in turn, and finally blown dry by nitrogen and baked at 120 °C for 120 s. Next, the AZ5214 (Merck, Darmstadt, Germany) photoresist is spin-coated, and the speed of the homogenizer is divided into three segments, with the speed of the first segment at 1000 r/min for 10 s, the second segment at 4000 r/min for 30 s, and the third segment at 1000 r/min for 10 s, baking 105 °C, 120 s. The first photolithography defines the waveguide shape and width. The exposure time is 6 s, the ratio of shadow solution is AZ400K (Merck, Darmstadt, Germany) developer-to-deionized water = 1:4, the development time is 30 s~40 s, and the firm film is 105 °C, 120 s. Wet etching is used to obtain the double channel and ridge waveguide, and the epitaxial wafer is submerged in the etching solution; after etching, it is rinsed with deionized water for 5 min and blown dry by nitrogen gas. The second lithography defines the ridge electrode injection area, the exposure time is 6 s, the ratio of shadow solution is developer-to-deionized water = 1:4, the development time is 30 s~40 s, and the firm film is 105 °C, 120 s. Then, the SiO_2 insulating layer is prepared, and the lift-off process is carried out because the photolithographic pattern left by the second lithography process has already been covered by the SiO_2, so it needs to be peeled off by the lift-off process. The third lithography defines the isolation slot, prepares the top ohmic electrode Ti/Pt/Au, and performs the lift-off process. Since the lithographic pattern left by the third lithography process has been covered by the ohmic contact layer, it is necessary to peel off the lithographic pattern covered by the ohmic contact layer with the lift-off process. Finally, the substrate was thinned and polished to 120 ± 10 μm, and the bottom ohmic electrode Ge/Au/Ni/Au was prepared.

This paper focuses on the QCL wet etching process. In the wet etching experiment, the etch rate can have an impact on the precise control of the etch depth, and the main influencing factors are the solution concentration and temperature. The concentration of the HBr solution was 48% (Macklin, Shanghai, China), the concentration of the HNO_3 (SCR, Shanghai, China) solution was 65–68%, and the deionized water (H_2O) configuration was $HBr:HNO_3:H_2O$ = 1:1:10 etching solution. The experimental temperature of the wet etching process was 20 °C.

The etching times taken for the experiment were 8 min, 9 min, 10 min, 11 min, and 12 min, totaling five time periods. The etching depth and lateral etching depth were measured by metallurgical microscope observation, and the variation curves of etching depth and lateral etching depth with time are shown in Figure 3. The etching rate of the sample with the ratio of $HBr:HNO_3:H_2O$ = 1:1:10 etching solution was about 0.6 μm/min, and the lateral etching rate was about 0.42 μm/min.

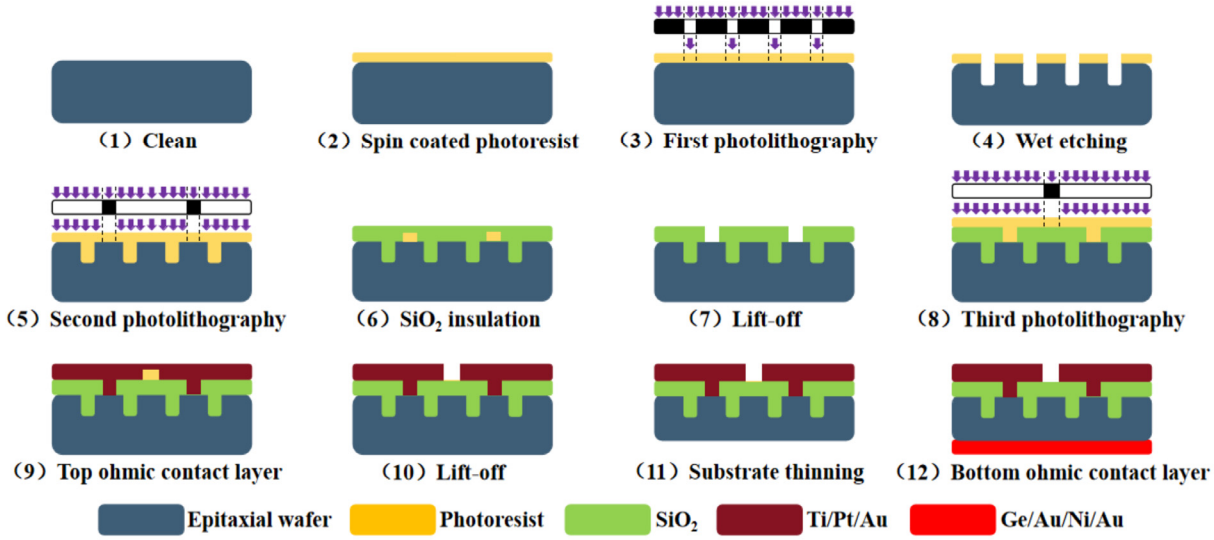

Figure 2. Process flow diagram of quantum cascade laser chip.

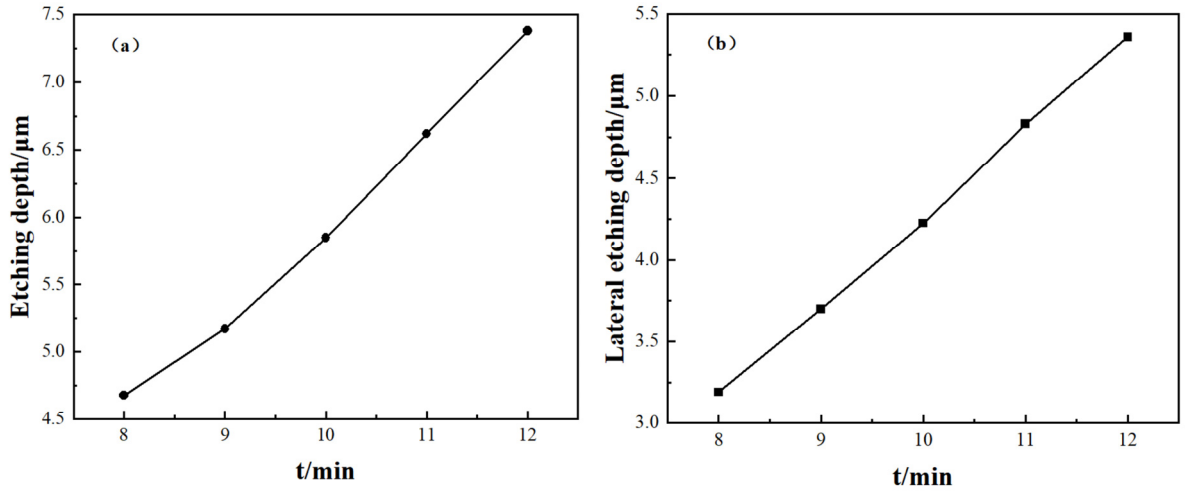

Figure 3. (**a**) The variation curve of the etching depth of the sample over time; (**b**) the variation curve of lateral etching depth of the sample over time.

3. Results and Discussion

3.1. Topographic Characterization

In this paper, a scanning electron microscope (JEOL, Tokyo, Japan) and a metallurgical microscope (Sunny Optical Technology, Yuyao, China) were used to characterize the etching morphology of the ridge waveguide. HBr:HNO_3:H_2O = 1:1:10 etching solution was used to etch the samples under the following experimental conditions: pre-baking 105 °C, 2 min, photolithography exposure time of 6 s, developer ratio AZ400K:deionized water = 1:4, developing time of 40 s, firm film 105 °C, 2 min, experimental temperature of 20 °C, etching solution ratio HBr:HNO_3:H_2O = 1:1:10, etching time of 11 min. As shown in Figure 3, the graphs of the etched samples were observed by a metallographic microscope. Figure 4a shows the ridge graphs on the surface of the etched samples (magnification 50×); the width of the ridge was measured to be 7.19 μm, the width of the side-etching was about 5.905 μm, and the clear channel and ridge table surface could be observed. Figure 4b shows the cross-section of the sample after etching (magnification 100×), which shows a "U"-shaped corrosion channel cross-section.

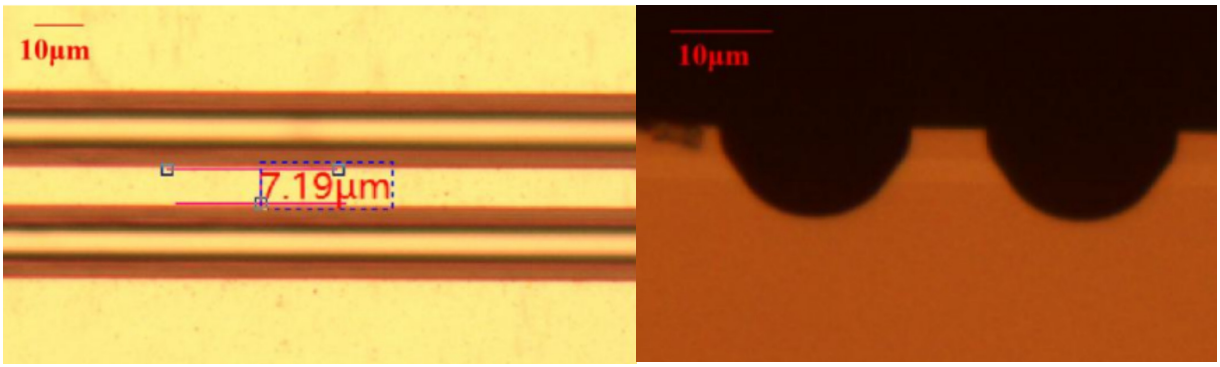

(**a**) (**b**)

Figure 4. Etched morphology observed under a metallurgical microscope: (**a**) ridge-shaped pattern on the surface of the sample after etching (50×); (**b**) cross-section pattern of sample after etching (100×).

As shown in Figure 5, the cross-section of the sample after etching with $HBr:HNO_3:H_2O$ = 1:1:10 etching solution was observed by SEM, and Figure 5a is the full-image SEM photo of the double channel ridge of the QCL, from which it can be observed that the double channel of the sample after wet etching exhibits a "U" shape, there is no lateral drilling, and the surface is flat and smooth. Figure 5b shows a magnified SEM photograph of the ridge-shaped region, and the red box region is the active region of the device.

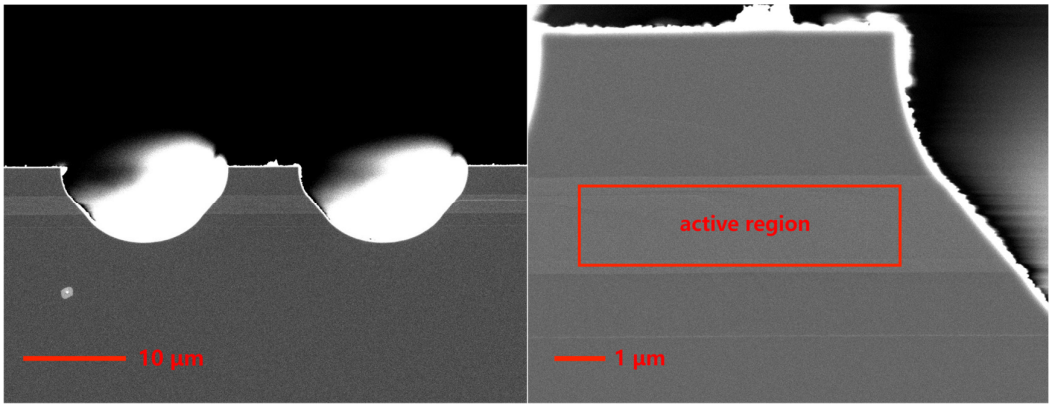

(**a**) (**b**)

Figure 5. SEM image of sample cross-section after etching ($HBr:HNO_3:H_2O$ = 1:1:10): (**a**) SEM image of the double channel ridge shape; (**b**) SEM photos of ridge-shaped areas.

3.2. Test Results of Chip Performance

P-I-V, emission spectrum, and reliability tests were performed on the InGaAs/InAlAs quantum cascade laser. The device has an injection strip width of 7 μm, a cavity length of 4 mm, and an operating temperature of 20 °C. The device operates in continuous mode (CW). The P-I-V test curves are shown in Figure 6a. The maximum continuous output power of the device is about 186 mW, the threshold current is about 0.4 A, and the threshold current density is about 1.428 kA/cm^2. The laser emission spectrum of the QCL in pulsed mode is shown in Figure 6b. The central wavelength is about 4424 nm, the side mode rejection ratio is 28 dB, and the full width and half height of the spectrum is 2 nm. As shown in Figure 6c, we performed an initial 72 h reliability test on the device. The device was placed on a test bench with a water-cooling system to maintain the operating temperature at 20 °C. The output power of the device gradually decreased from 186 mW to about 181 mW in the first 6 h under operating conditions of 0.6 A and 20 °C, and after this period, it remained stable at about 181 mW without exhibiting any obvious attenuation, and the reliability was stable.

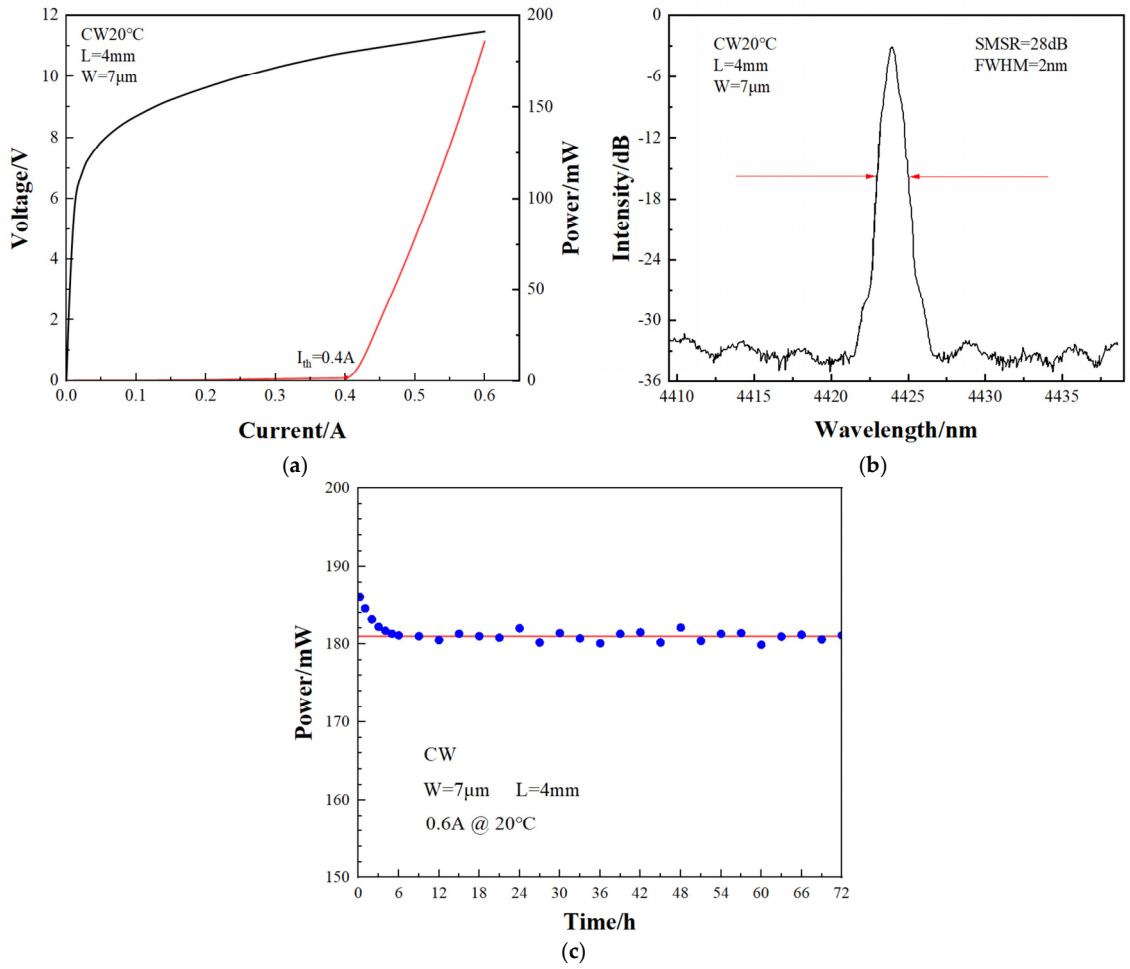

Figure 6. (**a**) P-I-V curve of the single-mode quantum cascade laser in continuous mode; (**b**) laser emission spectrum of the quantum cascade lasers in pulse mode; (**c**) 72 h reliability test of the quantum cascade laser.

4. Conclusions

The wet etching process of this experiment used a ratio of HBr:HNO_3:H_2O = 1:1:10 etching solution to etch the double channel ridge waveguide of InGaAs/InAlAs quantum cascade laser; the etching rate is about 0.6 μm/min, the etching rate is controllable, and the surface of the samples are all smooth. There is no undercutting effect, and the double channel presents a regular "U" shape. The final prepared quantum cascade laser bar width is 7 μm, the cavity length is 4 mm, the operating temperature is 20 °C, the device operates in continuous mode (CW), the maximum continuous output power of the device is about 186 mW, the threshold current is about 0.4 A, the threshold current density is about 1.428 kA/cm^2, the center wavelength of the device is about 4424 nm, the side-mode rejection ratio is 28 dB, and the spectral full-width-half-height is 2 nm. This study on the InGaAs/InAlAs quantum cascade laser etching process provides a good guarantee for the preparation of InGaAs/InAlAs quantum cascade lasers.

Author Contributions: Conceptualization, Q.W. and Y.Q.; methodology, Y.Z.; software, Z.L. and Z.Q.; validation, D.X. and Z.Z.; formal analysis, H.C.; investigation, Q.W. and Z.L.; resources, Y.Q.; data curation, Z.Q. and Y.Z.; writing—original draft preparation, Q.W.; writing—review and editing, G.L. and D.X.; visualization, L.Z.; supervision, Y.Q. and G.L.; project administration, Y.Q.; funding acquisition, L.L. All authors have read and agreed to the published version of the manuscript.

Funding: This research was supported by the National Natural Science Foundation of China (Nos. 62464006, 62274048, 62064004, and 62174046) and the Open Fund for Innovation and Entrepreneurship of College Students of Hainan Normal University (Nos. RSYH20231165818X and RSXH20231165809X).

Institutional Review Board Statement: Not applicable.

Informed Consent Statement: Not applicable.

Data Availability Statement: The original contributions presented in the study are included in the article material; further inquiries can be directed to the corresponding author.

Conflicts of Interest: The authors declare no conflicts of interest.

References

1. Razeghi, M.; Lu, Q.Y.; Bandyopadhyay, N.; Zhou, W.; Heydari, D.; Bai, Y.; Slivken, S. Quantum cascade lasers: From tool to product. *Opt. Express* **2015**, *23*, 8462–8475. [CrossRef] [PubMed]
2. Zhao, Y.; Zhang, J.; Liu, C.; Wang, L.; Liu, J.; Liu, F. Progress in mid-and far-infrared quantum cascade laser (invited). *Infrared Laser Eng.* **2018**, *47*, 8–17.
3. Kosterev, A.; Wysocki, G.; Bakhirkin, Y.; So, S.; Lewicki, R.; Fraser, M.; Tittel, F.; Curl, R.F. Application of quantum cascade lasers to trace gas analysis. *Appl. Phys. B* **2008**, *90*, 165–176. [CrossRef]
4. Meng, D.; Zhang, H.; Li, M.; Lin, W.; Shen, Z.; Zhang, J.; Fan, Z. Laser technology for direct IR countermeasure system. *Infrared Laser Eng.* **2018**, *47*, 150–159.
5. Isensee, K.; Kröger-Lui, N.; Petrich, W. Biomedical applications of mid-infrared quantum cascade lasers–a review. *Analyst* **2018**, *143*, 5888–5911. [CrossRef] [PubMed]
6. Pang, X.; Sirtori, C. Free space optical communication in the mid-IR for future long-range terrestrial and space applications. *Opt. Wirel. Commun. Technol.* **2023**, *2*, 9–12.
7. Faist, J.; Capasso, F.; Sirtori, C.; Sivco, D.L.; Hutchinson, A.L.; Cho, A.Y. Continuous wave operation of a vertical transition quantum cascade laser above T = 80 K. *Appl. Phys. Lett.* **1995**, *67*, 3057–3059. [CrossRef]
8. Hofstetter, D.; Beck, M.; Aellen, T.; Faist, J. High-temperature operation of distributed feedback quantum-cascade lasers at 5.3 μm. *Appl. Phys. Lett.* **2001**, *78*, 396–398. [CrossRef]
9. Evans, A.; Yu, J.S.; Slivken, S.; Razeghi, M. Continuous-wave operation of λ∼4.8 μm quantum-cascade lasersat room temperature. *Appl. Phys. Lett.* **2004**, *85*, 2166–2168. [CrossRef]
10. Lu, X.; Liu, F.; Liu, J.; Jin, P.; Wang, Z. Room temperature operation of strain-compensated 5.5 μm quantum cascade lasers. *Chin. J. Semi.* **2005**, *26*, 2267–2270.
11. Slivken, S.; Yu, J.S.; Evans, A.; David, J.; Doris, L.; Razeghi, M. Ridge-width dependence on high-temperature continuous-wave quantum-cascade laser operation. *IEEE Photonics Technol. Lett.* **2004**, *16*, 744–746. [CrossRef]
12. Evans, A.; Darvish, S.R.; Slivken, S.; Nguyen, J.; Bai, Y.; Razeghi, M. Buried heterostructure quantum cascade lasers with high continuous-wave wall plug efficiency. *Appl. Phys. Lett.* **2007**, *91*, 071101. [CrossRef]
13. Bai, Y.; Darvish, S.R.; Slivken, S.; Zhang, W.; Evans, A.; Nguyen, J.; Razeghi, M. Room temperature continuous wave operation of quantum cascade lasers with watt-level optical power. *Appl. Phys. Lett.* **2008**, *92*, 101105. [CrossRef]
14. Bai, Y.; Bandyopadhyay, N.; Tsao, S.; Slivken, S.; Razeghi, M. Room temperature quantum cascade lasers with 27% wall plug efficiency. *Appl. Phys. Lett.* **2011**, *98*, 181102. [CrossRef]
15. Zhang, J.; Liu, F.; Wang, L.; Chen, J.; Zhai, S.; Liu, J.; Wang, Z. High performance surface grating distributed feedback quantum cascade laser. *IEEE Photonics Technol. Lett.* **2013**, *25*, 686–689. [CrossRef]
16. Pang, L.; Cheng, Y.; Zhao, W.; Tan, S.; Guo, Y.; Li, B.; Wang, J.; Zhou, D. Mid-infrared quantum cascade laser grown by MOCVD at 4.6 μm. *Infrared Laser Eng.* **2022**, *51*, 189–194.
17. Fei, T.; Zhai, S.; Zhang, J.; Lu, Q.; Zhuo, N.; Liu, J.; Wang, L.; Liu, S.; Jia, Z.; Li, K.; et al. 3 W continuous-wave room temperature quantum cascade laser grown by metal-organic chemical vapor deposition. *Photonics* **2023**, *10*, 47. [CrossRef]
18. Bewley, W.; Canedy, C.; Kim, C.S.; Kim, M.; Lindle, J.R.; Abell, J.; Vurgaftman, I.; Meyer, J. Ridge-width dependence of midinfrared interband cascade laser characteristics. *Opt. Eng.* **2010**, *49*, 111116. [CrossRef]
19. Wittmann, A. High-Performance Quantum Cascade Laser Sources for Spectroscopic Applications. Ph.D. Thesis, ETH Zurich, Zurich, Switzerland, 2009.

Disclaimer/Publisher's Note: The statements, opinions and data contained in all publications are solely those of the individual author(s) and contributor(s) and not of MDPI and/or the editor(s). MDPI and/or the editor(s) disclaim responsibility for any injury to people or property resulting from any ideas, methods, instructions or products referred to in the content.